physica status solidi rrl
www.pss-rapid.com

Check for updates

TiN_x and TiO_x/TiN_x Barrier Layers for Al-Based Metallization of Passivating Contacts in Si Solar Cells

Benjamin Gapp, Heiko Plagwitz, Giso Hahn, and Barbara Terheiden*

A solution is presented for Ag-free contacting of passivating contacts for crystalline Si-based solar cells. In particular, a Ti-based diffusion barrier layer is introduced between the polycrystalline-Si of the passivating contact and standard screen-printed Al-paste, in order to prevent Al/Si alloying during contact sintering. This solution enables contact formation with industrial standard Al-pastes while maintaining high surface passivation quality of the underlying passivating contact. Metallization-induced implied open circuit voltage losses remain below 10 mV, with values > 720 mV before metallization. Contact resistivity values are below 3 Ωcm on average at substrate peak firing temperatures of 700 °C. This approach provides an alternative to Ag-based contact electrodes, while still maintaining high surface passivation quality and enabling low contact resistivity through the use of a conductive barrier layer. Thermal stability of the diffusion barrier and the impact of layer properties on its functionality are investigated. The impact of a TiO_x seed layer on diffusion barrier layer orientation is examined. Seed layer dependent properties, such as crystal orientation, are analyzed with X-ray diffraction. TiN_x layer orientation changes with introduction of the TiO_x seed layer, enabling a higher peak firing window. Diffusion profiles of Si, Al, and Ti are investigated via secondary-ion mass spectrometry.

1. Introduction

Solar cell concepts with passivating contacts, for example tunnel oxide passivated contacts cells, allow for high open-circuit voltages and currently achieve above 26% power conversion efficiency[1,2] with theoretically possible efficiencies up to 28.7%[3]. However, they use Ag electrodes as primary metal contacts for both polarities. Considering increasing photovoltaic deployment roadmaps and related projections of Ag consumption,[4,5] a large reduction of Ag consumption per watt peak produced is necessary with regard to the limited Ag supply, e.g., by applying alternative metals for contact formation. Al-based contact setups, in which alloying of Si and Al is typical, have been used extensively in Si-based solar cell concepts in the past (e.g., passivated emitter and rear cells (PERC)).[6,7] However, In order to maintain the surface passivation quality of a passivating contact comprised of SiO_x and n-type polycrystalline Si ((n) poly-Si:P) while still achieving low series resistance contributions from a conventional Al-paste for PERC applications, a barrier layer would be required that effectively prevents interaction between Al and poly-Si, but still allows for a low contact resistance. Ti-based layers, such as stoichiometric TiN, have been shown to act as a diffusion barrier against Al up to 55 °C[8–10] and Si up to 80 °C[11] for longer durations (30 min). TiO_x coatings deposited by atomic layer deposition have been used in photovoltaics before as passivation layers[12] while TiO_xN_y layers have been used as electron-selective contacts.[13] Al contact formation with low surface passivation losses, allowing for high implied open-circuit voltages (iV_{oc}), has lately been achieved by using TiN_x barrier layers by the authors.[14] In this work, a sputtered thin TiO_x layer is introduced as a buffer/seed layer underneath the layer stack comprised of TiN_x and intrinsic amorphous Si ((i)a-Si). A detailed look into the layer structure will be performed by analyzing X-ray diffraction (XRD) peaks after firing, and depth-resolved elemental composition changes within the layers will be analyzed by secondary-ion mass spectrometry (SIMS). Both TiN_x and TiO_x barrier systems can be deposited with the use of chemical vapor deposition[15–17]. In particular, plasma-enhanced chemical vapor deposition (PECVD), which is commonly used in solar cell manufacturing lines, provides a high-throughput, scalable deposition technique enabling cost-effective implementation of Ti-based barrier layers in existing manufacturing lines.[18,19]

2. Experimental Section

Phosphorus (10 Ωcm) and boron-doped (1 Ωcm) diamond-wire cut Czochralski (Cz)-Si wafers were precut into $50 \times 50\,mm^2$ sample size. After saw-damage removal in potassium hydroxide (KOH) at 800 °C, samples were precleaned in an ozone and a piranha etch solution. Both steps were followed up by a short HF-dip. SiO_x was then thermally grown in an O_2 atmosphere at 625 °C for

B. Gapp, H. Plagwitz, G. Hahn, B. Terheiden
Department of Physics
University of Konstanz
Konstanz, Baden-Wuerttemberg 78467, Germany
E-mail: benjamin.gapp@uni-konstanz.de

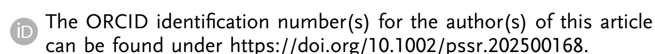
The ORCID identification number(s) for the author(s) of this article can be found under https://doi.org/10.1002/pssr.202500168.

© 2025 The Author(s). physica status solidi (RRL) Rapid Research Letters published by Wiley-VCH GmbH. This is an open access article under the terms of the Creative Commons Attribution License, which permits use, distribution and reproduction in any medium, provided the original work is properly cited.

DOI: 10.1002/pssr.202500168

Konstanzer Online-Publikations-System (KOPS)
URL: http://nbn-resolving.de/urn:nbn:de:bsz:352-2-120vawllj97kv5

about 10 min. All wafers were subsequently coated with an amorphous silicon (a-Si) layer (100 nm) on both sides in a PECVD process (direct plasma, Centrotherm) comprised of SiH_4, H_2, and PH_3 for in situ doping. The samples were then crystallized in a N_2 atmosphere at 920 °C for 30 min. After crystallization, the samples were coated on the front side with 75 nm hydrogenated silicon nitride (SiN_x:H) in a PECVD process (PECVD Oxford Plasmalab System 100, direct plasma). Barrier layer deposition on the rear side was then achieved at room temperature via reactive radio frequency magnetron sputtering (AJA ATC 2200) from a Ti target (5N) in an Ar/N plasma (ratio of gas fluxes $Ar/N_2 = 1:1$) for TiN_x and an Ar/O plasma (gas ratio $Ar/O_2 = 9:1$), with resulting layer thicknesses of $d_{TiOx} = 7$ nm and $d_{TiNx} = 35$ nm. Prior to each individual reactive sputtering step involving Ti, the Ti target was slowly ramped up to 600 W in an Ar plasma without reactive gases over the course of 600 s to prevent cross-contamination of reactants from the target surface. To prevent further oxidation of the barrier layers during subsequent steps at elevated temperatures, an additional a-Si layer was deposited via sputtering of a-Si target (5N) without a vacuum break. Samples with and without barrier layers were then screen-printed on the rear side with Al-paste, dried at 200 °C for 400 s. A full-area screen-printing mask was used to contact samples with an n-type base. The samples were then sintered (air) for contact formation in a rapid thermal annealing process in a belt furnace (firing) with the same initial heat-up ramp for all samples and varying substrate peak temperature (700–800 °C) (**Figure 1**).

This sample structure was then used to obtain cleaved cross-section SEM images. The Al metallization of the samples was etched back in 37% hydrochloric acid to enable photoconductance decay (PCD) measurements for passivation quality determination (evaluation of measurements at 1 sun), XRD for structural analysis of barrier and passivation layers, and SIMS measurements for element concentration analysis. PCD measurements were used to determine barrier layer function by evaluating and comparing implied open-circuit voltages. p-type base wafers were processed analogously up to printing, where they were selectively printed with an array of 60 µm × 9.5 mm electrodes for measurements using the transfer-length method in order to determine the impact of the barrier layer on contact resistivity between Al and the Ti-based barrier. Each set, consisting of 8 variably spaced electrodes, was printed within 1 of 20 laser-cut areas in order to electrically isolate it from the rest of the sample area. Optical properties were verified by ellipsometry (fit of layer thickness d based on Lorentz oscillator models), and sheet resistivity was analyzed by four-point-probe measurements and electrochemical capacitance–voltage.

3. Results

3.1. Firing Stability of Ti-Based Barrier Layers

In order to investigate barrier layer efficiency, we initially determined the dependence of the surface passivation quality using iV_{oc} values on peak substrate firing temperature. **Figure 2** shows iV_{oc} values obtained from two sets of samples, one set with TiO_x underneath the TiN_x and one without, each with and without full-area Al metallization after a firing process.

There is no discernible change in the iV_{oc} values of nonmetallized samples with changing peak firing temperature within the statistical fluctuations of the experiment. Most samples vary between −1 and +1% of the initial iV_{oc} during firing. When compared to unmetallized fired samples without barrier layers (not shown here), there is no significant surface passivation loss due to Ti-based layers alone. Additionally, samples without TiO_x show slightly higher iV_{oc} due to the reflective properties of

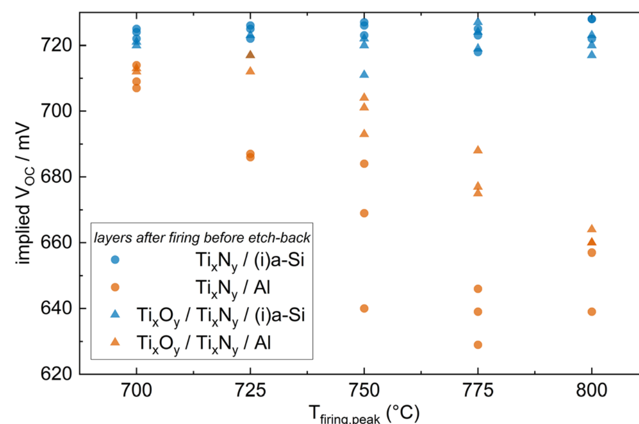

Figure 2. iV_{oc} values derived from PCD measurements dependent on peak sample temperature during firing with (orange) and without Al metallization (blue) of samples coated with Ti-based diffusion barriers with (circle) or without (triangle) TiO_x.

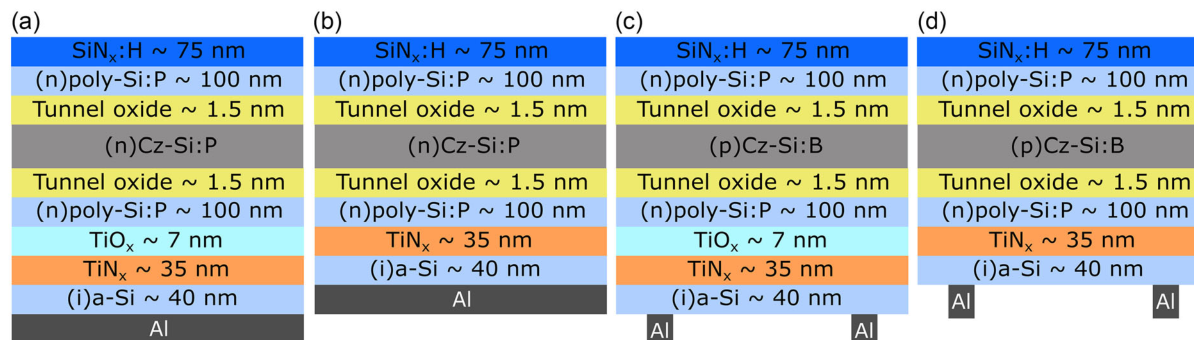

Figure 1. Schematic cross-sections of passivating contact samples with sputtered Ti-based diffusion barrier and screen-printed full-area a,b) and TLM c,d) Al metallization before firing.

© 2025 The Author(s). physica status solidi (RRL) Rapid Research Letters published by Wiley-VCH GmbH

TiN_x on the rear side. Overall, samples with Al metallization show lowered iV_{oc} values compared to samples without metallization, with a strong dependence on peak firing temperature. Losses occur more pronounced and at lower temperatures for samples without TiO_x. Samples with barrier layers containing TiO_x remain above 715 mV for firing temperatures up to 725° C, whereas samples without TiO_x show losses around 10 mV only at 700° C. As TiO_x is not a known diffusion barrier for Al, this effect of the TiO_x layer on the iV_{oc} and therefore barrier function of TiN_x is more likely to be based on its influence on the TiN_x structure.

3.2. Contact Resistivity of Ti-Based Barrier Stacks

Being an important factor for solar cell efficiency, the contribution of the contact resistivity by the Al contacts fired in this particular setup needs to be tested. Contact resistivity values obtained via transfer length method (TLM) on samples fired at substrate peak temperature of 700 °C are shown in **Figure 3**. Box plots were used to provide relevant statistical information such as mean (square), median and quartiles (lines in large square).

All samples were printed with a commercially available Al-paste intended for PERC back contact formation and fired at 700 °C substrate peak temperature. This was done to ensure contact formation while still maintaining diffusion barrier properties as well as enabling high surface passivation quality in a process comparable to typical solar cell processing. Finite element simulations of samples with a comparable structure show that these values are representative of the contact resistivity from the screen-printed Al to the TiN_x barrier layer, even though the sample structure used in this experiment does not follow standard TLM theory. The TLM measurements further show that the measured R_{sheet} of the sample shown lies between 20–30 Ω/sq, which is below both $R_{Sheet,TiNx}$ and $R_{Sheet,poly\text{-}Si}$, suggesting parallel conduction in both TiN_x and (n)poly-Si:P. This indicates that the TiN_x/(n)poly-Si:P interface does not limit current transport significantly, since it is likely that both the TiN_x barrier layer and (n) poly-Si:P conduct equally. Contact resistivity values for samples without TiO_x are lower on average, while the distribution of measurement values is similar compared to samples with TiO_x.

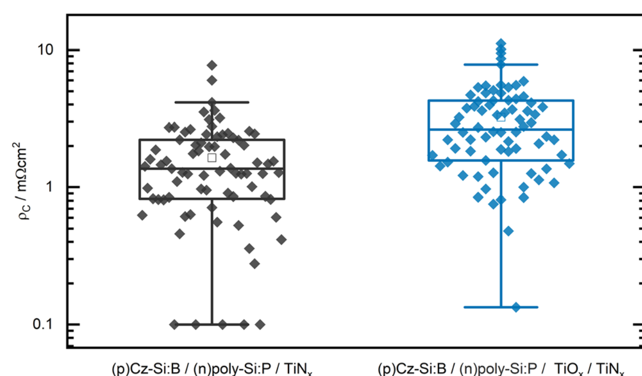

Figure 3. Contact resistivity values based on measurements using the TLM method for samples fired at 700 °C after Al printing on barrier stacks without (black) and with TiO_x (blue).

3.3. Structural and Elemental Analysis of Barrier Layers

To understand how the diffusion barrier impacts contact formation and prevents surface passivation losses, a more detailed look is necessary. **Figure 4** shows cross-sections of (n)poly-Si:P layers contacted with Al-paste after firing at 700 °C. Figure 4a shows a sample without a diffusion barrier, while Figure 4b–d shows a sample containing a TiO_x/TiN_x diffusion barrier stack in different magnifications.

Areas in which Al/Si alloying occurred during contact sintering can be clearly seen in 4a. In these areas, the passivating SiO_x/poly-Si contact stack is completely dissolved. This alloying can be prevented with the use of a barrier layer, as can be seen in Figure 4b–d. Additionally, large grains can be seen within the Ti-based barrier, in Figure 4d, with a typical grain size being comparable to the layer thickness. A diffusion of Ti and Al from and through the grain boundaries between these grains might be the cause of the passivation changes shown in Figure 2. The barrier layers appear intact even when in direct contact with Al-paste beads, preventing Si–Al exchange and interaction on a large scale.

An elemental analysis of selected samples from Figure 2, fired at 700, 725, and 800 °C, via SIMS was performed. Element concentrations of Ti and Al were measured against a-Si monitor signal in dependence on sputtering depth. The respective signals of Si, Al, and Ti, obtained from a mass spectrometer during sputtering vertically into the sample, can be found in **Figure 5**a–c, respectively. Two measurement curves of each sample are shown in Figure 5. An additional sample without screen-printed Al and a high temperature step has been measured in order to distinguish sputtering-based drive-in effects during the measurement from diffusion during firing. All measurements are normalized on the x-axis to the Si bulk /SiO_x interface to facilitate comparison of different diffusion effects. Signal intensity stemming from additional sources needs to be taken into account. With the given Ti target purity of 5N, the measured amount of Al (10^{18}–10^{19} cm^{-3}) is not expected to be introduced into sputtered Ti-containing layers. This contamination is therefore traced back to an internal source within the sputtering machine. However, the incorporated Al does not seem to have a negative influence on the diffusion barrier properties concerning the iV_{oc} measured in this work. Similar experiments, where Al was deliberately incorporated into a sputtered layer stack, have been performed[11] and even led to an improvement of mechanical layer properties. However, these Al sources can influence the intensity of the Al signal during the subsequent measurement process of the underlying layers. This needs to be taken into consideration when interpreting the SIMS measurement. Passivation losses, as seen in Figure 2, are therefore more likely the result of the smaller-scale diffusion of defect species Al and possibly Ti toward the passivating contact interface, and not large-scale Si–Al interaction. In this case, the Al might already have been introduced during sputtering from an internal source within the machine.

With the thermal budget during firing being the main driving factor of the diffusion of both Al and Ti, the substrate peak firing temperature during firing has a major influence. No conclusive evidence of an influence of substrate peak temperature on Si

© 2025 The Author(s). physica status solidi (RRL) Rapid Research Letters published by Wiley-VCH GmbH

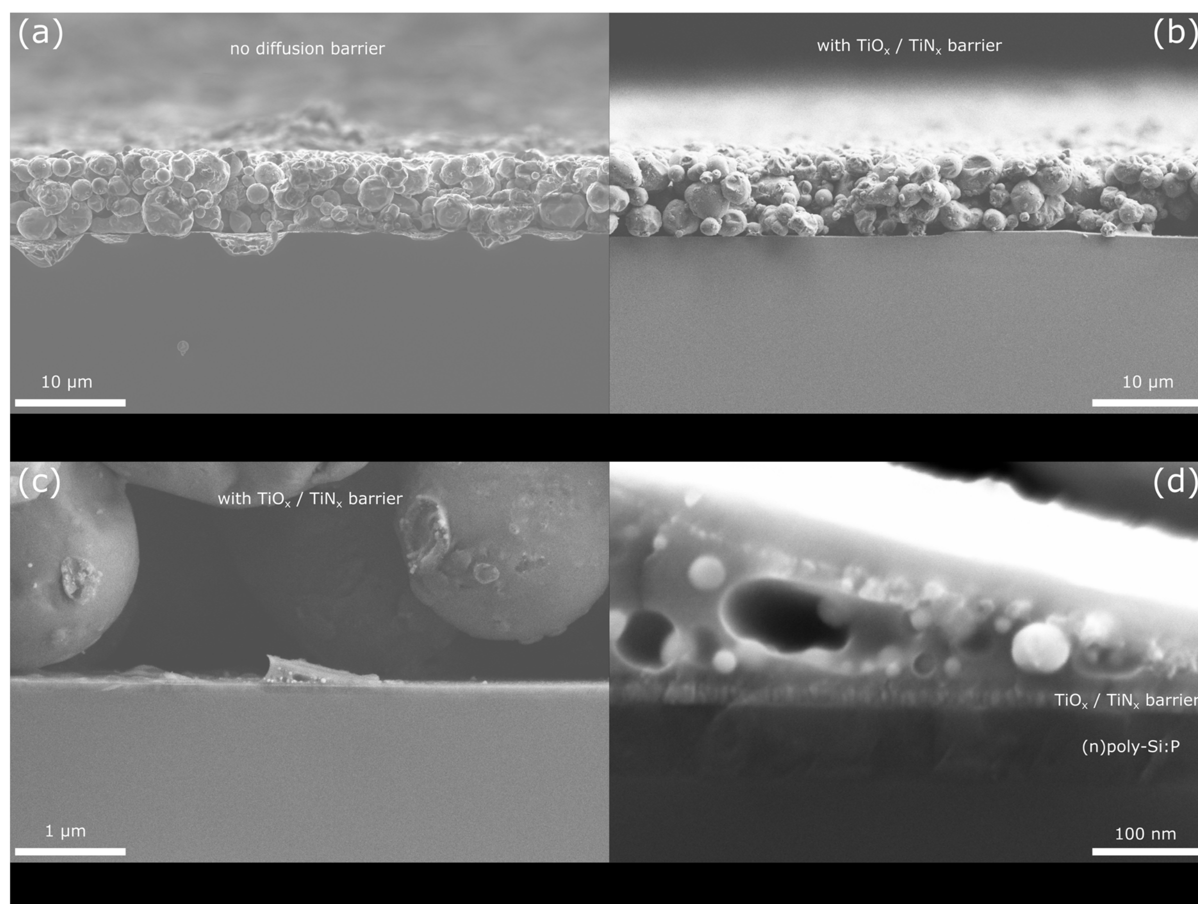

Figure 4. SEM-overview of a cross-section of samples as described in Figure 2, fired at 700 °C. a) No diffusion barrier layer is applied, whereas in b–d), sputtered TiO_x and TiN_x barrier layers are used as diffusion barriers (different magnifications).

diffusion within the TiN_x layer can be found from SIMS measurements. The reference sample shows a significant Ti-signal in the layer below the TiN_x barrier, which is likely the result of a sputtering-based drive-in that occurs during measuring. Since this drive-in depends on the layer composition, it can be explained by the different sputtering rates and structure of the layers, which were not fired. At 700 °C substrate peak temperature, the TiO_x layer does seem to have some influence on the Al diffusion, whereas Ti diffusion is similar for both layer types. This similarity between samples without firing and those fired at 700 °C shows that there is no measurable firing-based in-diffusion, further implying the stability of the layers during firing at 700 °C. The signals of Ti and Al at and below the SiO_x interface are below the SIMS detection limit for samples fired at 700 °C. Ti and Al concentration stemming from in-diffusion toward the poly-Si layer increases and is correlated with the decrease in passivation quality when increasing substrate peak temperature from 700 to 800 °C.

Comparing both layers at 800 °C, it is evident that the diffusion of both Ti and Al is stronger in layers containing TiO_x. This shows an influence of the TiO_x layer on the breakdown threshold of the diffusion barrier at this temperature. At 800 °C, even though the metals Ti and Al are found in and below the passivating contact in high quantities, some passivation quality is retained. This can be explained by a possible Al-BSF (back surface field) formation. It is possible that at this stage, the metals act as dopant material near the surface of the sample, and, depending on how they are incorporated into the Si crystal, might act as a surface field preventing recombination on a lower level than the passivating contact. Taking into account the Ti drive-in during SIMS measurement, it can be concluded that no significant amount detrimental to surface or bulk passivation quality is introduced during firing up to 725 °C. A sample fired at 725 °C without TiO_x shows similar elemental concentrations for both Ti and Al within the barrier and (n)poly-Si:P layer when compared to samples fired at 700 °C. Therefore, the decrease in passivation quality starting at 725 °C for samples without TiO_x cannot be explained solely by in-diffused Ti quantities shown in the SIMS measurement due to limited resolution. It is possible that lower concentrations of, in particular, Ti also impact passivation quality by introducing recombination defect levels.

Figure 6a shows the diffraction pattern obtained by grazing incidence X-ray diffraction (GI-XRD) of samples shown in Figure 2 at 1° incidence angle. The diffraction pattern shows reflexes typical for poly/c-Si [111 220 311 400] and stoichiometric

© 2025 The Author(s). physica status solidi (RRL) Rapid Research Letters published by Wiley-VCH GmbH

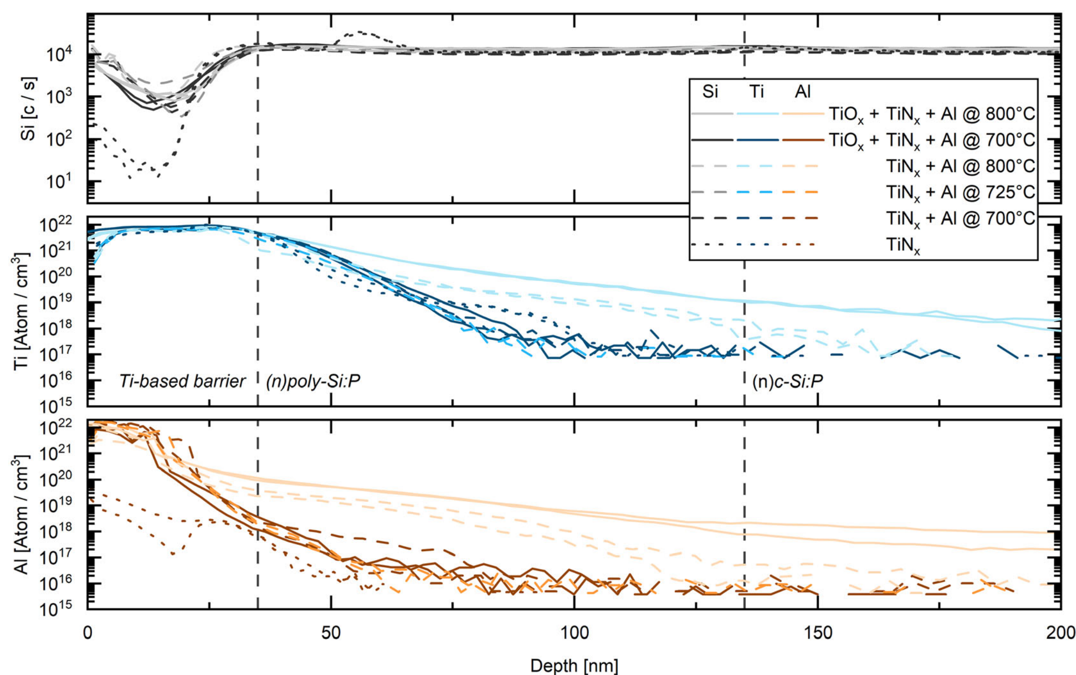

Figure 5. SIMS intensity profiles of Si (gray, top), Ti (blue, middle), and Al (orange, bottom) depending on sputtering sample depth of fired samples with metallization after Al-bulk etch-back.

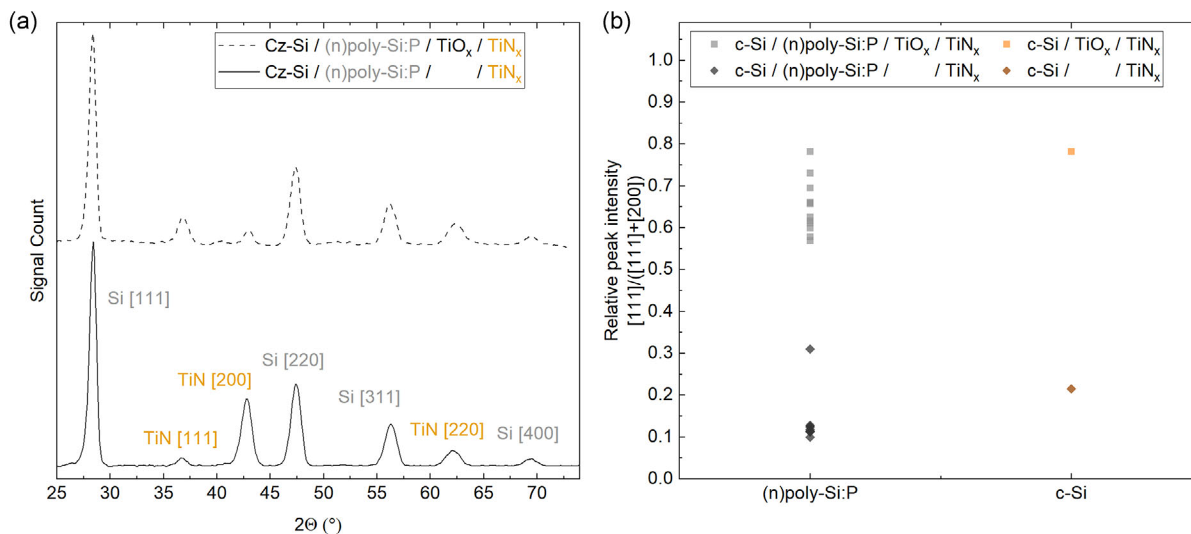

Figure 6. a) GI-XRD scan of Al-printed and fired ($T_{peak} = ^{700}$ °C) samples with barrier layers on (n)poly-Si:P samples after etch-back. The barrier is comprised of either TiN_x (compact line) or both TiO_x and TiN_x (dashed line), shown on top. Peaks are depicted in gray for Si [111 220 311 400] and yellow for TiN_x [111 200 220]. b) Relative peak intensity of the [111] TiN_x peak for both fired (gray) barrier layers on (n)poly-Si:P and unfired reference samples where barrier layers are deposited directly on c-Si (brown and yellow).

TiN [111 200 220]. A [111] oriented TiN crystal is typical when Ar is used as sputtering gas, but other orientations are possible if the nitrogen content (in this work, equal gas flows $Q_{Ar} : Q_{N_2} = 1$) in the plasma is high enough.[20] No significant diffraction reflexes could be determined for Ti or nonstoichiometric TiN, indicating near-stoichiometric growth during sputtering, or TiO_x, which can likely be attributed to its small thickness and likely amorphous growth structure. The Si reflexes are comparable to nonmetallized and nonfired (n)poly-Si:P for both samples, which indicates no major structural changes in the (n)poly-Si:P layer due to either barrier deposition, screen-printing, and firing. However, there are slight differences in the TiN [111 200] reflexes for samples with and without TiO_x. The height of both [111 200] reflexes changes depending on the layer sequence,

© 2025 The Author(s). physica status solidi (RRL) Rapid Research Letters published by Wiley-VCH GmbH

which is further illustrated in Figure 6b. The TiO_x [111] reflex is more prominent for samples with TiO_x, whereas stronger[200] reflexes are measured without the buffer layer. As a typically face centered cubic (FCC) structured crystal,[21,22] the TiN [111]orientation presents the highest planar density. Additionally, due to its typically NaCl-like FCC structure,[23] TiN presents itself as layered with only one atom species facing the surface in this configuration. When comparing relative peak intensity in Figure 6b, the impact of both contact firing and the crystallinity of the underlying Si (poly-Si layer compared to monocrystalline Si wafer surface) on the structure of TiN_x is much lower than the impact of the presence of a TiO_x buffer layer.

4. Discussion

Using a Ti-based barrier layer prevents significant interaction between Si and Al, as indicated by the maintained passivation quality after firing, which is further consolidated by scanning electron microscopy (SEM) images. Since overall passivation quality decreases with increasing peak firing temperature on samples with metallization, temperature-dependent effects, such as diffusion, need to be taken into account. Samples with additional TiO_x buffer layer show, independent of peak firing temperature, higher passivation quality. This correlates well with their overall different structural orientation, with TiN_x on underlying TiO_x being more preferentially oriented in the more dense [111] direction than without the TiO_x buffer layer. In addition to that, samples without Al metallization do not exhibit any dependence on firing temperature or the use of an underlying TiO_x in terms of passivation quality (Figure 2).

Having an Al metallization on the barrier layer is crucial for the interactions shown in the depth-resolved elemental analysis, indicating an interaction of Al with the barrier layer and its components, causing the passivation quality change described above. The diffusion of elements Ti and Al toward the poly-Si layer correlates with the passivation quality decrease between 700 and 800 °C, with higher concentration shown for samples fired at higher substrate peak temperature. When comparing samples with and without TiO_x at the same substrate peak temperatures, however, Ti and Al concentration curves are very similar at 700 and 725 °C. At 700 °C, both sample types exhibit similar diffusion profiles, which fit the iV_{oc} results. This shows that the effects of TiO_x only become significant at 725 °C and upwards, increasing the thermal stability, and therefore higher possible thermal budget while maintaining high surface passivation (iV_{oc}). It is possible that the different preferential orientation of the TiN_x caused by the TiO_x buffer layer is responsible for the increased surface passivation quality and thus barrier function obtained with the TiO_x/TiN_x barrier stack. Also, an effect of oxygen on Al diffusion in TiN_x has been studied where it is postulated that O binds to diffusing Al to form Al_2O_3,[24] which in turn prevents further Al diffusion through pinholes and grain boundaries between columns.

It is possible that Al is introduced during sputtering, and the aforementioned effect occurs during deposition. Moreover, although the TiO_x/TiN_x barrier layer stack shows a higher thermal stability than the TiN_x single layer barrier up to 725–750 °C, we find higher Ti and Al concentrations after firing at 800 °C. A different effect seems to occur or become dominant for samples fired at 800 °C. An influence of the Al on barrier layer structure during firing is likely, possibly destabilizing the TiN_x layer, which in turn might enable more Al to diffuse in or through the barrier layer. A similar development on TiN with a longer firing time has been shown by Lee et al.[11] This does not explain, however, why the samples with TiO_x exhibit higher in-diffusion of Ti and Al while maintaining higher passivation quality even after firing at 775 and 800 °C, as in particular Ti acts as a defect species which is expected to be detrimental to passivation[25–27]. A possible explanation of this might be the formation of an Al-BSF, enabling surface passivation at this level (640 mV), although no large–scale interaction could be found in SEM cross-section pictures, suggesting a very thin Al-BSF. Further analysis on the defect formation of in-diffused Ti and Al in samples fired at these temperatures is necessary in order to understand their effect on surface passivation and bulk recombination. In particular, the lifetime impact of Ti and Ti–Al interaction in Si requires further examination.

5. Conclusion

We have shown the efficacy of Ti-based layers as a diffusion barrier for passivating contacts to be used in crystalline Si solar cells. An additional seed layer, such as TiO_x, can be used to optimize the TiN_x barrier function further, increasing passivation quality and enabling higher substrate peak temperatures during firing of around 725–750 °C. Typical Si–Al interaction, such as alloying and the formation of a eutectic melt, is prevented, leaving to a small extent solid phase diffusion of Si, Ti, and Al as an exchange mechanism. Elemental analysis shows that Si, Al, and Ti diffusion, as well as the thermal barrier breakdown threshold, are correlated with the TiN_x layer structure, with higher amounts of [111] oriented grains proving beneficial.

Acknowledgements

Part of this work was funded by the German ministry of economy and climate action (FKZ 03EE1106B). The content is the responsibility of the authors. The authors would like to thank Barbara Rettenmaier for technical support and Thomas Pernau of centrotherm international AG for PECVD depositions.

Open Access funding enabled and organized by Projekt DEAL.

Conflict of Interest

The authors declare no conflict of interest.

Author Contributions

Benjamin Gapp: conceptualization (equal); data curation (lead); formal analysis (lead); investigation (lead); writing—original draft (lead); methodology (equal); visualization (equal); validation (equal). **Heiko Plagwitz**: conceptualization (equal); project administration (equal); data curation (equal); formal analysis (equal); investigation (equal); methodology (equal); supervision (equal); validation (equal); writing—review and editing (equal). **Giso Hahn**: resources (equal); supervision (equal); writing—review and editing (equal). **Barbara Terheiden**: conceptualization (equal);

© 2025 The Author(s). physica status solidi (RRL) Rapid Research Letters published by Wiley-VCH GmbH

funding acquisition (lead); project administration (lead); resources (equal); supervision (equal); validation (equal); writing—review and editing (equal).

Data Availability Statement

The data that support the findings of this study are available from the corresponding author upon reasonable request.

Keywords

aluminum, diffusion barriers, passivating contacts

Received: April 25, 2025
Revised: May 20, 2025
Published online: June 30, 2025

[1] M. Green, E. Dunlop, J. Hohl-Ebinger, M. Yoshita, N. Kopidakis, X. Hao, *Prog. Photovolt.: Res. Appl.* **2021**, *29*, 3.
[2] F. Haase, C. Hollemann, S. Schäfer, A. Merkle, M. Rienäcker, J. Krügener, R. Brendel, R. Peibst, *Sol. Energy Mater. Sol. Cells.* **2018**, *186*, 184.
[3] W. Long, S. Yin, F. Peng, M. Yang, L. Fang, X. Ru, M. Qu, H. Lin, X. Xu, *Sol. Energy Mater. Sol. Cells.* **2021**, *231*, 111291.
[4] Y. Zhang, M. Kim, L. Wang, P. Verlinden, B. Hallam, *EES* **2021**, *14*, 5587.
[5] B. Hallam, M. Kim, Y. Zhang, L. Wang, A. Lennon, P. Verlinden, P. P. Altermatt, P. R. Dias, *Prog. Photovolt.: Res. Appl.* **2023**, *31*, 598.
[6] G. Fischer, M. Müller, S. Steckemetz, R. Köhler, F. Lottspeich, F. Wolny, C. Koch, T. Roth, M. Kipping, H. Neuhaus, E. Schneiderlöchner, *Energy Procedia.* **2015**, *77*, 515.
[7] M. Wittmer, *JVSTA* **1985**, *74*, 105.
[8] A. Sherman, *JES* **1990**, *137*, 1892.
[9] G. Grigorov, K. Grigorov, M. Stoyanova, J. Vignes, J. Langeron, P. Denjean, *Appl. Phys. A* **1993**, *57*, 195.
[10] K. Grigorov, G. Grigorov, M. Stoyanova, J. Vignes, J. Langeron, P. Denjean, J. Perriere, *Appl. Phys. A* **1992**, *55*, 502.
[11] H. J. Lee, R. Sinclair, P. Li, B. Roberts, *J. Appl. Phys.* **1999**, *86*, 3096.
[12] J. Cui, T. Allen, Y. Wan, J. Mckeon, C. Samundsett, D. Yan, X. Zhang, Y. Cui, Y. Chen, P. Verlinden, A. Cuevas, *Sol. Energy Mater. Sol. Cells.* **2016**, *158*, 115.
[13] X. Yang, Y. Lin, J. Liu, W. Liu, Q. Bi, X. Song, J. Kang, F. Xu, L. Xu, M. N. Hedhili, D. Baran, X. Zhang, T. D. Anthopoulos, S. De Wolf, *Adv. Mater.* **2020**, *32*, 32.
[14] B. Gapp, H. Plagwitz, G. Hahn, B. Terheiden, *SiPV Conf. Proc.* **2024**, *2*, https://doi.org/10.52825/siliconpv_v2i_1303
[15] J. S. Kim, B.-H. Jun, E. J. Lee, C. Y. Hwang, W. J. Lee, *Thin Solid Films* **1997**, *292*, 124.
[16] I. S. Lee, J. W. Kim, C. J. Youn, S. K. Park, Y. B. Hahn, *Korean J. Chem. Eng.* **1996**, *13*, 473.
[17] K. Davis, K. Jiang, C. Demberger, H. Zunft, D. Habermann, W. Schoenfeld, *2013 IEEE 39th Photovoltaic Specialists Conference (PVSC).*, IEEE, Piscataway **2013**, p. 1.
[18] J. I. Polzin, F. Feldmann, B. Steinhauser, M. Hermle, S. Glunz, *AIP Conference Proceedings*, AIP publishing SiPV, Leuven **2018**, 1999, p. 040018.
[19] F. Feldmann, T. Fellmeth, B. Steinhauser, H. Nagel, D. Ourinson, S. Mack, E. Lohmüller, J. I. Polzin, J. Benick, A. Richter, A. Moldovan, M. Bivour, F. Clement, J. Rentsch, M. Hermle, S. Glunz, *2019, 36th European Photovoltaic Solar Energy Conf. and Exhibition*, WIP, Marseille **2019**, pp. 304-308
[20] R. Banerjee, R. Chandra, P. Ayyub, *Thin Solid Films* **2002**, *405*, 64.
[21] W. Lengauer, *J. Alloys Compd.* **1992**, *186*, 293.
[22] Z. Chen, *J. Chem. Phys.* **1993**, *98*, 231.
[23] L. Toth, *Transition Metal Carbides And Nitrides*, Academic Press, New York, London **1971**.
[24] W. Sinke, G. Frijlink, F. Saris, *APL* **1985**, *47*, 471.
[25] J. Schmidt, N. Thiemann, R. Bock, R. Brendel, *J. Appl. Phys.* **2009**, *106*, 9.
[26] M. Mehler, A. Zuschlag, M. Trempa, T. Buck, G. Hahn, *in Proc. 40th EUPVSEC*, WIP, Munich **2023**, 020027-001 - 020027-004.
[27] B. Paudyal, K. McIntosh, D. Macdonald, *J. Appl. Phys.* **2009**, *105*, 12.

© 2025 The Author(s). physica status solidi (RRL) Rapid Research Letters published by Wiley-VCH GmbH